DOI: 10.1002/ejic.200800778

Inter- and Intrachain Spin-Transition Processes in One-Dimensional Polynuclear Iron(III) Complexes of *N*,*N*′-Ethylenebis(acetylacetonylideneimine) Bridged by 1,3-Bis(4-pyridyl)propane and 1,4-Bis(imidazolyl)butane

Shinya Imatomi,[a] Shingo Hashimoto,[a] and Naohide Matsumoto*[a]

Keywords: Iron / Spin crossover / Chain structures / Solid-state structures / Magnetic properties

Two one-dimensional (1D) polynuclear iron(III) complexes, $[Fe^{III}(acacen)(bpyp)]BPh_4$ (**1**) and $[Fe^{III}(acacen)(bimb)]BPh_4$ (**2**), were synthesized [acacen = *N*,*N*′-ethylenebis(acetylacetonylideneiminato); bpyp = 1,3-bis(4-pyridyl)propane; bimb = 1,4-bis(imidazolyl)butane]. Complexes **1** and **2** show gradual spin-crossover (SCO) behavior over a wide temperature range from 100 to 300 K and from 220 to higher than 350 K, respectively. The single-crystal X-ray structures of two complexes in the high-spin (HS), low-spin (LS), and the midpoint between HS and LS states were determined. Crystal structures of both complexes consist of two molecular units (Fe1 and Fe2), where complex **1** consists of two crystallographically independent 1D chains and complex **2** consists of one 1D chain involving two molecular units. At the temperature midway between the HS and LS states, the Fe–N bond lengths in the two units are different from each other. At the midpoint, complex **1** consists of alternately arrayed independent HS and LS chains, whereas complex **2** consists of alternately arrayed HS and LS units within a chain. The results demonstrate two different SCO mechanisms of a 1D complex, that is, SCO occurs in chain-by-chain fashion for **1** and in adjacent Fe units within a chain for **2**.

Introduction

Spin crossover (SCO) is the conversion between two or more spin states according to physical perturbations such as the temperature, pressure, and light irradiation. SCO complexes have attracted special attention from the viewpoints of basic coordination chemistry and possible applications as new electronic devices for molecular memory and molecular switches.[1] SCO behavior is driven by a change in metal–ligand distances and hence a change of the ligand-field strength. Although SCO behavior is essentially described as a phenomenon of a single molecule, a number of unusual SCO effects have been reported and rationalized by intermolecular interactions. Now it is well recognized that interaction between SCO sites is an important factor that governs SCO properties, such as the steepness of the spin transition, hysteresis, and the LIESST (light-induced excited-spin-state trapping) effect.[2]

Thus, the synthesis of SCO complexes exhibiting interactions between SCO sites is of current interest. During the last two decades, polymeric SCO complexes with bridging ligands,[3] binuclear SCO complexes,[4] and mononuclear SCO complexes exhibiting weak intermolecular interactions such as hydrogen bonding and π–π stacking[5] have been extensively investigated and show interesting SCO behavior. Nevertheless, the SCO transition seems to be strongly influenced in a complicated way by many secondary factors, and the detailed mechanism of SCO behavior is not perfectly understood.

In our previous papers,[6] to understand the mechanism of SCO transitions better, we studied a series of SCO mononuclear, binuclear, and one-dimensional (1D) iron(III) complexes with Schiff base ligands derived from diamine and salicylaldehyde derivatives, whereby the binuclear and 1D complexes were formed by linear bridging ligands such as 4,4′-bipyridine. Recently, we synthesized the isomorhous mononuclear and binuclear iron(III) complexes $[Fe^{III}L^1(meim)]BPh_4$ and $[Fe^{III}{}_2L^1{}_2(bimb)](BPh_4)_2$, and investigated the effect of nuclearity on the SCO behavior {H_2L = bis(3-methoxysalycylideneaminopropyl)amine, bimb = 1,4-bis-imidazolylbutane, meim = *N*-methylimidazole, BPh_4^- = tetraphenylborate}.[7] Herein, we report the synthesis, magnetic properties, and crystal structures of two 1D polynuclear SCO iron(III) complexes, $[Fe^{III}(acacen)(bpyp)]BPh_4$ (**1**) and $[Fe^{III}(acacen)(bimb)]BPh_4$ (**2**) [acacen is the equatorial quadridentate ligand *N*,*N*′-ethylenebis(acetylacetonylideneiminato)]. Two linear bridging ligands, 1,3-bis(4-pyridyl)propane (bpyp) and 1,4-bis(imidazolyl)butane (bimb), were used. Because the two complexes showed different SCO transition processes, we report herein the inter- and intrachain spin-transition processes in 1D polynuclear iron(III) complexes. Studies of **1** were in part reported previously in a communication.[8]

[a] Department of Chemistry, Faculty of Science, Kumamoto University,
Kurokami 2-39-1, Kumamoto 860-8555, Japan
Fax: +81-96-342-3390
E-mail: naohide@aster.sci.kumamoto-u.ac.jp

Results and Discussion

Magnetic Properties of Complex 1

The magnetic susceptibilities of crystalline samples of $[Fe^{III}(acacen)(bpyp)]BPh_4$ (**1**) were measured in the temperature range 5–350 K at a sweep rate of 1 K min^{-1} under a 0.5 T applied magnetic field. The sample was quickly cooled from room temperature to 5 K, and the magnetic susceptibilities were first measured in warming mode from 5 to 350 K and then measured in cooling mode from 350 to 5 K. Plots of $\chi_M T$ vs. T for the warming and cooling modes, together with the derivative of the $\chi_M T$ vs. T curve, are shown in Figure 1 (χ_M is the molar magnetic susceptibility per Fe atom, and T is the absolute temperature). The $\chi_M T$ vs. T plots show no difference in the cooling and warming modes and reveal a reversible, gradual, and almost complete spin crossover (SCO) between the HS (S = 5/2) and LS (S = 1/2) states. At 350 K, the $\chi_M T$ value of 3.85 cm^3 K mol^{-1} is slightly lower than the expected value of 4.37 cm^3 K mol^{-1} for the HS iron(III) species (S = 5/2, g = 2.00). Upon lowering the temperature from 350 K, the $\chi_M T$ value gradually decreases and reaches a plateau value of 0.58 cm^3 K mol^{-1} below 100 K; this value is comparable with the typical value of 0.4–0.5 cm^3 mol^{-1} K for LS iron(III) complexes (S = 1/2). As evidenced by the X-ray analysis, the transition curve is a combination of different processes centered at different temperatures, and the transition temperature (high-spin fraction = 0.5) is roughly approximated by the derivative of $\chi_M T$ vs. T. The derivative of the $\chi_M T$ vs. T curve shows a broad peak with the maximum at 180 K, demonstrating gradual SCO behavior over a wide temperature range of around 200 K. At the temperature of the maximum (180 K), the populations of HS and LS species should be equal.

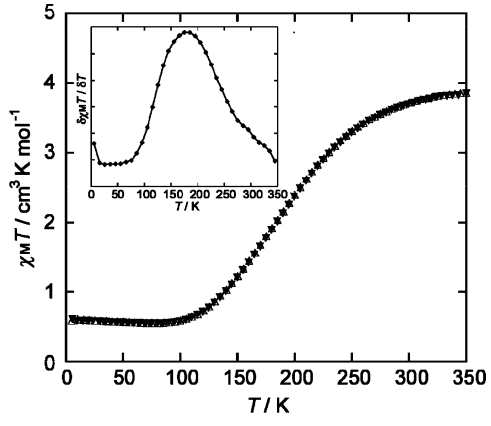

Figure 1. Plots of $\chi_M T$ per Fe atom vs. T for $[Fe^{III}(acacen)(bpyp)]BPh_4$ (**1**) in warming (△) and cooling (▼) modes; inset: derivative of the $\chi_M T$ vs. T curve.

The present SCO behavior can be compared with that of mononuclear SCO iron(III) complexes containing similar donor atoms. In comparison with mononuclear iron(III) complexes that exhibit complete SCO behavior, for example $[Fe^{III}py(L)]BPh_4$, complex **1** shows more gradual SCO behavior over a wide temperature range, probably because of the flexible 1D chain structure. Mononuclear iron(III) complexes with pyridine derivatives as the axial ligand show SCO behavior over a wide temperature range of approximately 150 K, which is typical for isolated SCO iron(III) complexes.

Structural Description of Complex 1

Single-crystal X-ray structures of complex **1** were determined at 296, 180, and 108 K, at which temperatures the complex is in the HS state, in an intermediate state between the HS and LS states, and in the LS state, respectively. The intermediate temperature of 180 K was obtained from the maximum of the derivative of the $\chi_M T$ vs. T curve. Table 1 shows the crystallographic data. The cell parameters are similar at each of the three temperatures, and the space group remains the same, $Pca2_1$ (No. 29), which indicates there is no phase change during the spin transition, as expected from the gradual SCO behavior. The cell volume decreases by 3.8% from 8447(3) Å^3 at 296 K in the HS state to 8137(2) Å^3 at 108 K in the LS state.

Table 1. X-ray crystallographic data for complex **1**.

Formula	$C_{49}H_{52}BFeN_4O_2$		
Molecular mass	795.63		
Temperature	296 K	180 K	108 K
Crystal system	orthorhombic	orthorhombic	orthorhombic
Space group	$Pca2_1$ (No. 29)	$Pca2_1$ (No. 29)	$Pca2_1$ (No. 29)
a [Å]	25.132(2)	24.839(7)	24.708(3)
b [Å]	13.925(4)	13.914(3)	13.893(2)
c [Å]	24.136(3)	23.883(5)	23.704(3)
V [Å^3]	8447(3)	8255(3)	8137(2)
Z	8	8	8
$\rho_{calcd.}$ [g cm^{-3}]	1.251	1.280	1.299
μ [cm^{-1}]	4.01	4.10	4.16
R_1 [$I > 2.0\sigma(I)$][a]	0.067	0.072	0.071
wR_2 (all data)[b]	0.150	0.204	0.211

[a] $R_1 = \Sigma||F_o| - |F_c||/\Sigma|F_o|$. [b] $wR_2 = \{\Sigma[w(F_o^2 - F_c^2)^2]/\Sigma w(F_o^2)^2\}^{1/2}$.

The crystal structure consists of two crystallographically independent molecular units of $[Fe^{III}(acacen)(bpyp)]BPh_4$. The molecular structures of the cations at 180 K are shown in Figure 2 together with the atom numbering scheme. Each iron(III) ion (Fe1 and Fe2) assumes a similar octahedral coordination environment with the N_4O_2 donor atoms. The equatorial coordination sites are occupied by the N_2O_2 donor atoms of the quadridentate ligand acacen and two axial positions are occupied by two pyridyl N atoms of 1,3-bis(4-pyridyl)propane, which functions as a bridging ligand. One of two axial sites of a Fe^{III} ion (Fe1) is coordinated by N3 of a bpyp and another axial site is coordinated by N4* of the adjacent bpyp ligand. As a result, the complex forms a 1D chain. The crystal consists of two crystallographically independent chains, whereby the Fe1 chain and Fe2 chain are alternately stacked. Figure 3 shows the crystal structure of the 1D chains running along the a axis; the Fe1 chain is shown in black and the Fe2 chain is shown in gray. There are no hydrogen bonds and no π–π interactions between the chains.

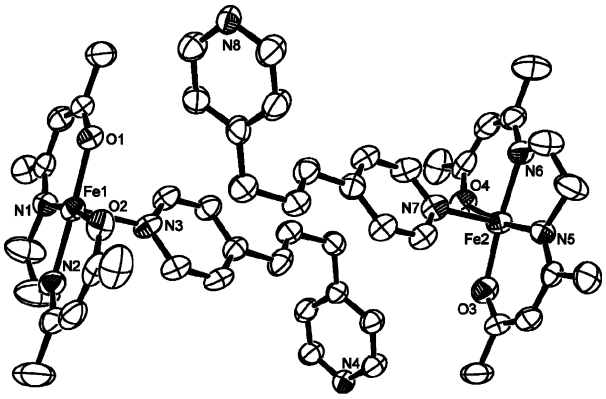

Figure 2. Molecular structures of the cations of the two molecular units of **1** at 180 K.

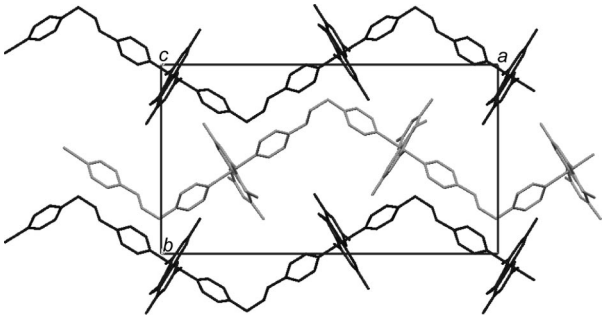

Figure 3. Crystal packing diagram of **1** at 180 K. Hydrogen atoms and BPh_4^- ions are omitted for clarity. HS (Fe1) and LS (Fe2) chains running along the *a* axis are stacked alternately.

The coordination bond lengths of SCO complexes are indicative of the spin state. Relevant bond lengths are given in Table 2 (the same atom numbering scheme is used for all temperatures). At 108 and 296 K, the dimensions around the coordination sphere of the Fe1 chain are not different from those of the Fe2 chain. But at 180 K, the dimensions of the Fe1 chain are significantly different from those of the Fe2 chain. In the LS state at 108 K, the axial Fe–N bond lengths at the Fe1 and Fe2 sites are similar to each other, and the average bond lengths (Fe1–N 1.974 Å; Fe2–N 1.976 Å) are consistent with two Fe^{III} sites in the LS state. At 180 K, the axial Fe–N bond lengths at the Fe1 and Fe2 sites are 1.996 and 2.065 Å, respectively, which demonstrates that two Fe sites are in different spin states. At 296 K, the axial Fe–N bond lengths at the Fe1 and Fe2 sites are 2.110 and 2.141 Å, respectively, which demonstrates that the two iron(III) sites are almost in the HS states. These data imply that the Fe2 site converts from the LS into the HS state at a lower temperature than the Fe1 site.

Table 2. Coordination bond lengths [Å] of **1** at 296, 180, and 108 K.

Bond	296 K	180 K	108 K
Fe(1)–O(1)	1.919(2)	1.888(2)	1.892(2)
Fe(1)–O(2)	1.919(2)	1.898(2)	1.908(2)
Fe(1)–O(av)	1.919	1.893	1.900
Fe(1)–N(1)	2.040(2)	1.938(2)	1.902(2)
Fe(1)–N(2)	2.044(2)	1.938(2)	1.918(2)
Fe(1)–N(3)	2.190(2)	2.056(2)	2.037(2)
Fe(1)–N(4)	2.169(2)	2.052(2)	2.037(2)
Fe(1)–N(av)	2.110	1.996	1.974
Fe(2)–O(3)	1.921(2)	1.914(2)	1.903(2)
Fe(2)–O(4)	1.918(2)	1.892(2)	1.906(2)
Fe(2)–O(av)	1.920	1.903	1.900
Fe(2)–N(5)	2.055(2)	1.991(2)	1.912(2)
Fe(2)–N(6)	2.060(2)	1.997(2)	1.914(2)
Fe(2)–N(7)	2.215(2)	2.141(2)	2.048(2)
Fe(2)–N(8)	2.235(2)	2.131(3)	2.028(2)
Fe(2)–N(av.)	2.141	2.065	1.976

Magnetic Properties of Complex 2

The $\chi_M T$ vs. T plots of complex **2** for the warming and cooling modes, together with the derivative of the $\chi_M T$ vs. T curve, in the temperature range 5–350 K are shown in Figure 4. The $\chi_M T$ vs. T plots reveal gradual SCO and show a small difference between the cooling and warming modes. This difference could be due to the loss of the crystal solvent, as evidenced by thermogravimetric analysis (TGA). On heating the sample at a rate of 2 K min^{-1}, the weight gradually decreases up to 380 K as a result of the loss of crystal solvent molecules, and at higher temperature the TGA curve decreases abruptly. At 350 K, the highest temperature of the present magnetic measurements, the $\chi_M T$ value of 2.87 cm^3 K mol^{-1} is lower than the expected value of 4.35 cm^3 K mol^{-1} for a HS iron(III) species (S = 5/2, g = 2.00). Upon lowering the temperature from 350 K, the $\chi_M T$ value decreases and reaches a plateau value of 0.48 cm^3 K mol^{-1} below 200 K, which is as expected for a LS iron(III) species (S = 1/2). The derivative of the $\chi_M T$ vs. T curve shows the inflection point at 296 K, and at this temperature the population of HS/LS species is equal.

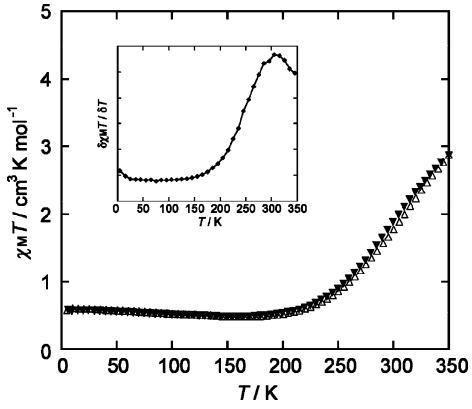

Figure 4. The $\chi_M T$ per Fe vs. T plots of $[Fe^{III}(acacen)(bimb)]BPh_4$ (**2**) in the warming (△) and cooling (▼) modes, together with the derivative of the $\chi_M T$ vs. T curve in inset.

Structural Description of Complex 2

The single-crystal X-ray structures of complex **2** were determined at three temperatures; at 370 K: the highest temperature of the present X-ray diffraction study, at 296 K: the inflection point of $\chi_M T$ vs. T curve and the midpoint between the HS and LS states, and at 190 K, where the

complex is in the LS state. Table 3 lists the crystallographic data. The cell parameters at the three temperatures are similar and have the same space group $P\bar{1}$ (No. 2), which indicates there is no phase change during the spin transition, as expected from the gradual SCO behavior. The cell volume decreases by 3.5% from 4433(2) Å^3 at 370 K to 4276(2) Å^3 at 190 K in the LS state.

Table 3. X-ray crystallographic data for complex **2**.

Formula	$C_{46.5}H_{54}BFeN_6O_{2.5}$		
Molecular mass	803.63		
Temperature	370 K	296 K	190 K
Crystal system	triclinic	triclinic	triclinic
Space group	$P\bar{1}$ (No.2)	$P\bar{1}$ (No.2)	$P\bar{1}$ (No.2)
a [Å]	16.044(4)	15.967(5)	15.907(5)
b [Å]	16.247(6)	16.186(4)	16.115(4)
c [Å]	17.034(5)	16.882(5)	16.716(6)
α [°]	88.49(1)	88.21(1)	88.16(1)
β [°]	87.15(1)	87.18(1)	86.84(1)
γ [°]	89.93(1)	89.96(1)	89.97(1)
V [Å^3]	4433(2)	4356(2)	4276(2)
Z	4	4	4
$\rho_{calcd.}$ [g cm^{-3}]	1.204	1.225	1.248
μ [cm^{-1}]	3.844	3.912	3.985
R_1 [$I > 2.0\sigma(I)$][a]	0.0673	0.056	0.1028
wR_2 (all data)[b]	0.2296	0.128	0.3421

[a] $R_1 = \Sigma||F_o| - |F_c||/\Sigma|F_o|$. [b] $wR_2 = \{\Sigma[w(F_o^2 - F_c^2)^2]/\Sigma w(F_o^2)^2\}^{1/2}$.

The crystal structure consists of two molecular units of [Fe^{III}(acacen)(bimb)]BPh$_4$ and one methanol molecule as a unique crystallographic unit. The molecular structures of the cations of the two molecular units at 296 K are shown in Figure 5 together with the atom numbering scheme. The equatorial coordination sites are occupied by an acacen ligand and the two axial positions are occupied by imidazole N atoms of bridging bimb ligands. Figure 5 shows that within a chain, Fe1 and Fe2 sites are bridged by a bimb ligand and alternately arrayed. There are two bimb ligands in the crystallographic unit, and the geometries of the butyl moieties in two bridging ligands differ: one bimb ligand forms a *gauche-anti-anti* geometry, and the other is of *gauche-anti-gauche* type.

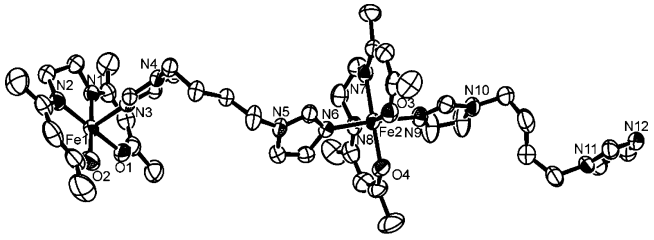

Figure 5. Molecular structure of the cation of **2** at 296 K. Two bridging ligands assume different conformations (from the left side; *gauche-anti-anti* type and *gauche-anti-gauche* type).

The coordination bond lengths of SCO complexes are indicative of the spin state. Relevant bond lengths are given in Table 4 (the same atom numbering scheme positions is used for all temperatures). In the LS state at 190 K, the average distances of the Fe–N and Fe–O bond of the Fe1 and Fe2 sites are almost same; the average bond lengths (Fe1–N 1.959 Å, Fe1–O 1.893 Å; Fe2–N 1.953 Å, Fe2–O 1.905 Å) are consistent with the two iron(III) sites in the LS states. At 370 K near the HS state, the average bond lengths of the Fe1 and Fe2 sites (Fe1–N 2.070 Å, Fe1–O 1.928 Å; Fe2–N 2.075 Å, Fe2–O 1.930 Å) are similar to each other and longer than the corresponding values at 190 K. In contrast, at 296 K, the average bond lengths of the Fe1 site (Fe1–N 1.995 Å, Fe1–O 1.894 Å) are distinctly different from those of the Fe2 site (Fe2–N 2.025 Å, Fe2–O 1.909 Å). The data at 296 K indicate that the Fe1 and Fe2 sites are close to the LS and HS states, respectively.

Table 4. Relevant bond lengths [Å] of complex **2** at 370, 296, and 190 K.

Bond	370 K	296 K	190 K
Fe(1)–O(1)	1.928(2)	1.902(2)	1.898(3)
Fe(1)–O(2)	1.928(3)	1.886(2)	1.888(3)
Fe(1)–O(av.)	1.928	1.894	1.893
Fe(1)–N(1)	2.030(2)	1.949(2)	1.910(3)
Fe(1)–N(2)	2.031(3)	1.961(2)	1.935(3)
Fe(1)–N(3)	2.103(2)	2.032(2)	1.993(3)
Fe(1)–N(12)	2.117(3)	2.040(2)	1.998(3)
Fe(1)–N(av.)	2.070	1.995	1.959
Fe(2)–O(3)	1.929(2)	1.907(2)	1.900(3)
Fe(2)–O(4)	1.930(2)	1.910(2)	1.910(2)
Fe(2)–O(av.)	1.930	1.909	1.905
Fe(2)–N(7)	2.021(2)	1.980(2)	1.910(3)
Fe(2)–N(8)	2.050(2)	1.991(2)	1.910(3)
Fe(2)–N(6)	2.114(2)	2.060(2)	1.993(3)
Fe(2)–N(9)	2.115(3)	2.069(3)	1.998(3)
Fe(2)–N(av.)	2.075	2.025	1.953

A crystal-packing diagram at 296 K is shown in Figure 6, in which the Fe1 moiety in the HS state is shown in black and the Fe2 moiety in the LS state is shown in gray. The Fe1 site in the HS state (black) and the Fe2 site in the LS state (gray) are bridged by a bimb ligand and the HS and LS species are alternately arranged within a chain.

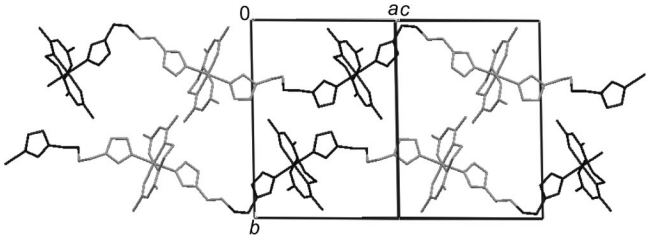

Figure 6. Crystal packing diagram of **2** at 296 K. Hydrogen atoms, BPh_4^- ions, and methanol molecules are omitted for clarity. HS (Fe1, black) and LS (Fe2, gray) species are bridged by a bimb ligand and are alternately arranged within a chain.

Concluding Remarks

In this work, two types of 1D polynuclear SCO iron(III) complexes, [Fe^{III}(acacen)(bpyp)]BPh$_4$ (**1**) and [Fe^{III}-(acacen)(bimb)]BPh$_4$ (**2**), are reported, in which planar iron(III) species {Fe^{III}(acacen)}$^+$ are bridged axially by a linear bridging ligand at two terminal sites to give a 1D chain structure. Both complexes show gradual SCO behav-

ior over a wide temperature range, which suggests that this chain structure is unsuitable for gaining steep SCO behavior and hysteresis. Crystal structures of both complexes consist of two molecular units (Fe1 and Fe2). Complex **1** consists of two crystallographically independent 1D chains, and complex **2** consists of a chain with two molecular units. At the temperature midway between the HS and LS states, complex **1** consists of alternately arrayed independent HS and LS chains, whereas complex **2** consists of alternately arrayed HS and LS units within a chain. The results demonstrate two different SCO mechanisms for the 1D SCO complexes, that is, SCO occurs in chain-by-chain fashion for **1** and in adjacent units within a chain for **2**.

Experimental Section

Materials: All reagents and solvents in the syntheses were of reagent grade and were used without further purification. [Fe^{III}Cl(acacen)] was prepared according to a literature procedure.[9] 1,3-Bis(4-pyridyl)propane (bpyp) was purchased from Tokyo Chemical Industry Ltd., and 1,4-bis(imidazolyl)butane dihydrate (bimb·$2H_2O$) was prepared according to a literature procedure.[10]

[Fe^{III}(acacen)(bpyp)]BPh_4 (1): To a solution of [Fe^{III}Cl(acacen)] (157 mg, 0.5 mmol) in methanol (30 mL) was added a solution of 1,3-bis(4-pyridyl)propane (100 mg, 0.5 mmol) in methanol (20 mL). The mixture was warmed and stirred for 10 min and then filtered. The filtrate was added to a solution of sodium tetraphenylborate ($NaBPh_4$) (171 mg, 0.5 mmol) in methanol (20 mL) at ambient temperature. The resulting solution was left to stand overnight, during which time black crystals suitable for X-ray analysis precipitated, which were collected by suction filtration, washed with methanol, and dried. Complex **1** shows thermochromism in the solid state, changing from purple at room temperature to green at liquid-nitrogen temperature, which is suggestive of SCO behavior. $C_{49}H_{52}BFeN_4O_2$ (795.63): calcd. C 73.97, H 6.59, N 7.04; found C 73.54, H 6.72, N 7.10. IR (KBr pellet): $\nu_{C=N}$(imine) 1610, ν_{B-C}(BPh_4^-) 730, 709 cm^{-1}.

[Fe^{III}(acacen)(bimb)]BPh_4·0.5CH_3OH·0.5H_2O (2): To a solution of [Fe^{III}Cl(acacen)] (157 mg, 0.5 mmol) in methanol (30 mL) was added a solution of 1,4-bis(imidazolyl)butane dihydrate (110 mg, 0.5 mmol) in methanol (20 mL). The mixture was warmed and stirred for 10 min and then filtered. The filtrate was added to a solution of $NaBPh_4$ (171 mg, 0.5 mmol) in methanol (10 mL). The resulting solution was left to stand overnight, during which time black crystals precipitated, which were collected by suction filtration, washed with methanol, and dried. Complex **2** shows thermochromism in the solid state, changing from purple at room temperature to green at liquid-nitrogen temperature, which is suggestive of SCO behavior. $C_{46}H_{52}BFeN_6O_2$·0.5CH_3OH·0.5H_2O (812.63): calcd. C 68.73, H 6.82, N 10.34; found C 68.63, H 6.60, N 10.68. IR (KBr pellet): $\nu_{C=N}$(imine) 1580, ν_{B-C}(BPh_4^-) 737, 704 cm^{-1}.

Physical Measurements: Elemental C, H, and N analyses were carried out at the Center for Instrumental Analysis of Kumamoto University. Infrared spectra were recorded on a Nicolet Avatar 370 DTGS (Thermo Electron Corporation) spectrometer by using KBr disks at ambient temperature. Magnetic susceptibilities were measured with a MPMS-5S SQUID (Quantum Design) in the temperature range 5–350 K under an applied magnetic field of 0.5 T. Calibration was performed with palladium metal. Corrections for diamagnetism were applied using Pascal's constants.

Crystallographic Data Collection and Structure Analyses: The X-ray diffraction data were collected by using a Rigaku R-Axis Rapid imaging plate diffractometer with graphite-monochromated Mo-K_α radiation. The temperature of the crystal was maintained at the selected value within an accuracy of ±2 K by means of a Rigaku cooling device. A crystal of complex **1** (black block crystal, $0.31 \times 0.23 \times 0.37$ mm) and a crystal of complex **2** (black block crystal, $0.41 \times 0.38 \times 0.37$ mm) were used. All calculations were performed with the CrystalStructure software package.[11] The structures were solved by direct methods[12] and expanded using the Fourier technique.[12] Hydrogen atoms were fixed at calculated positions and refined by using a riding model. Although the thermal analysis of **2** indicated the existence of methanol and water molecules, the crystal solvent water molecule was not clearly located in the Fourier difference map. CCDC-600523, -600524, -600525 (complex **1** at 296, 180, and 108 K, respectively) and 696665, -696666, -696667 (complex **2** at 190, 296, and 370 K, respectively) contain the supplementary crystallographic data for this paper. These data can be obtained free of charge from The Cambridge Crystallographic Data Centre via www.ccdc.cam.ac.uk/data_request/cif.

Acknowledgments

This work was supported in part by a Grant-in-Aid for Scientific Research (No. 16205010) from the Ministry of Education, Science, Sports, and Culture of Japan. We thank Miss. Kikue Nishiyama at the Center for Instrumental Analysis of Kumamoto University for the elemental analyses.

[1] a) E. König, *Prog. Inorg. Chem.* **1987**, *35*, 527–623; b) H. A. Goodwin, *Coord. Chem. Rev.* **1976**, *18*, 293–325; c) P. Gütlich, A. Hauser, H. Spiering, *Angew. Chem. Int. Ed. Engl.* **1994**, *33*, 2024–2054; d) P. Gütlich, H. A. Goodwin, *Spin Crossover in Transition Metal Compounds I–III*, Topics in Current Chemistry, vol. 233–235, Springer, New York, **2004**; e) S. Decurtins, P. Gütlich, C. P. Köhler, A. Hauser, *Chem. Phys. Lett.* **1984**, *105*, 1–4; f) O. Kahn, J. C. Martinez, *Science* **1998**, *279*, 44–48; g) P. J. van Koningsbruggen, Y. Garcia, O. Kahn, L. Fournes, H. Kooijman, A. L. Spek, J. G. Haasnoot, J. Moscovici, K. Provost, A. Michalowicz, F. Renz, P. Gütlich, *Inorg. Chem.* **2000**, *39*, 1891–1900; h) J.-A. Real, E. Andres, M. C. Munoz, M. Julve, T. Granier, T. A. Bousseksou, F. Varret, *Science* **1995**, *268*, 265–267.

[2] a) S. Hayami, Z. Gu, M. Shiro, A. Einaga, A. Fujishima, O. Sato, *J. Am. Chem. Soc.* **2000**, *122*, 7126–7127; b) Y. Sunatsuki, Y. Ikuta, N. Matsumoto, M. Kojima, S. Iijima, S. Hayami, Y. Maeda, S. Kaizaki, F. Dahan, J.-P. Tuchagues, *Angew. Chem. Int. Ed.* **2003**, *42*, 1614–1618; c) Y. Ikuta, M. Ooidemizu, Y. Yamada, S. Osa, N. Matsumoto, S. Iijima, Y. Sunatsuki, M. Kojima, F. Daha, J.-P. Tuchagues, *Inorg. Chem.* **2003**, *42*, 7001–7017; d) H. Hagiwara, S. Hashimoto, N. Matsumoto, S. Iijima, *Inorg. Chem.* **2007**, *46*, 3136–3143; e) M. Yamada, H. Hagiwara, H. Torigoe, N. Matsumoto, M. Kojima, F. Dahan, J.-P. Tuchagues, N. Re, S. Iijima, *Chem. Eur. J.* **2006**, *12*, 4536–4549.

[3] a) Y. Garcia, O. Kahn, L. Rabardel, B. Chansou, L. Salmon, J.-P. Tuchagues, *Inorg. Chem.* **1999**, *38*, 4663–4670; b) E. Breuning, M. Ruben, J.-M. Lehn, F. Renz, Y. Garcia, V. Ksenofontov, P. Gütlich, E. Wegelius, K. Rissanen, *Angew. Chem. Int. Ed.* **2000**, *39*, 2504–2507; c) N. Moliner, C. Munoz, S. Letard, X. Solans, N. Menendez, A. Goujon, F. Varret, J. A. Real, *Inorg. Chem.* **2000**, *39*, 5390–5393.

[4] K. Murray, *Eur. J. Inorg. Chem.* **2008**, 3101–3121.

[5] a) S. Hayami, Z. Gu, M. Shiro, A. Einaga, A. Fujishima, O. Sato, *J. Am. Chem. Soc.* **2000**, *122*, 7126–7127; b) S. Hayami, G. Z. Gu, M. Shiro, A. Einaga, A. Fujishima, O. Sato, *J. Am.*

Chem. Soc. **2001**, *123*, 11644–11650; c) S. Dorbes, L. Valade, J.-A. Real, C. Faulmann, *Chem. Commun.* **2005**, 69–71; d) Z. J. Zhong, J.-O. Tao, Z. Yu, C.-Y. Dun, Y.-J. Liu, X.-Z. You, *J. Chem. Soc., Dalton Trans.* **1998**, 327–328; e) J.-F. Le'tard, P. Guionneau, E. Codjovi, O. Lavastre, G. Bravic, D. Chasseau, O. Kahn, *J. Am. Chem. Soc.* **1997**, *119*, 10861–10862; f) R. Boca, M. Boca, L. Dihan, K. Falk, H. Fuess, W. Haase, R. Jarosciak, B. Papankova, F. Renz, M. Vrbova, R. Werner, *Inorg. Chem.* **2001**, *40*, 3025–3033.

[6] a) R. Kitashima, S. Imatomi, M. Yamada, N. Matsumoto, Y. Maeda, *Chem. Lett.* **2005**, *34*, 1388–1389; b) K. Tanimura, R. Kitashima, N. Bréfuel, M. Nakamura, N. Matsumoto, S. Shova, J.-P. Tuchagues, *Bull. Chem. Soc. Jpn.* **2005**, *78*, 1279–1289.

[7] S. Imatomi, T. Sato, T. Hamamatsu, R. Kitashima, N. Matsumoto, *Bull. Chem. Soc. Jpn.* **2007**, *80*, 2375–2377.

[8] S. Imatomi, R. Kitashima, T. Hamamastu, M. Okeda, Y. Ogawa, N. Matsumoto, *Chem. Lett.* **2006**, *35*, 502–503.

[9] N. Matsumoto, S. Ohta, C. Yoshimura, S. Kohata, Y. Maeda, H. Okawa, A. Ohyoshi, *J. Chem. Soc., Dalton Trans.* **1985**, 2575–2584.

[10] W. Schtze, H. Schubert, *J. Prakt. Chem.* **1959**, *8*, 306.

[11] *CrystalStructure 3.8.2*, *Crystal Structure Analysis Package*, Rigaku and Rigaku/MSC, 9009 New Trails Drive, The Woodlands, Texas 77381-5209, USA.

[12] P. T. Beurskens, G. Admiraal, G. Beurskens, W. P. Bosman, R. de Gelder, R. Israel, J. M. M. Smits, *The DIRDIF-99 Program System*, Technical Report of the Crystallography Laboratory, University of Nijmegen, Nijmegen, The Netherlands, **1999**.

Received: August 5, 2008
Published Online: November 12, 2008

